



Full Length Article

The inhibiting effect and mechanisms of smart polymers on the transport of fluids throughout nano-channels

Yang Zhou^{a,b,1,*}, Jingshun Cai^b, Dongshuai Hou^c, Honglei Chang^{d,2,*}, Jiao Yu^c

^a School of Materials Science and Engineering, Southeast University, Nanjing 211189, China

^b State Key Laboratory of High Performance Civil Engineering Materials, Jiangsu Research Institute of Building Science Co., Nanjing 211103, China

^c Department of Civil Engineering, Qingdao University of Technology, Qingdao 266033, China

^d School of Qilu Transportation, Shandong University, Jinan 250002, China

ARTICLE INFO

Keywords:

Smart polymer
Molecular dynamics
Nano-channel
Ion transport
Concrete durability

ABSTRACT

The transport of ions throughout the nano-channels is vital to the performance of porous materials. Here, a novel smart polymer with both hydrophilic and hydrophobic components was designed by molecular dynamics to regulate the capillary penetration process in cement-based materials, which determines the overall durability. The polymer structure owns carboxyl groups at one end, which are strongly attracted by the surface of a cementitious matrix due to the high polarity, as well as several alkyl groups. The polymer chain acts like a unilateral gate, which is open (lie on the matrix surface) when the nano-pore is anhydrous. However, it can be closed rapidly (stand upright, vertical to the matrix), utilizing the hydrophobic groups to maximize the transport inhibiting effect once in contact with the advancing fluids. Furthermore, a fluid transport inhibitor was fabricated based on the above mechanisms and added to the concrete mixtures. The experimental results indicate after the incorporation of this inhibitor, the water adsorption amount and chloride ion migration rate of concrete experience a huge decrease, indicating a substantial enhancement in the durability of samples. The surface interactions interpreted here may also shed new light on the understandings of smart polymers and their applications onto various matrixes.

1. Introduction

The transport of water and ions throughout the nano-channels is vital to the overall performance of porous materials. The corrosion of reinforcing steels caused by the chlorides penetration throughout the concrete cover is considered as the main problem in the durability issues of reinforced concrete structures.[1,3] Calcium silicate hydrates (C-S-H), the main hydration product of ordinary Portland cement, contains large numbers of gel pores with several nanometers to several hundred nanometers, which provide the transport path for chloride ions. Reversely, the transport and adsorption behaviors of water and ions in those pores are vital to the strength developments, volume stability, and durability of cementitious materials.[3–8]³ Therefore, effective control on the transport of fluids through those nano-channels is in urgent demand.

So far, researchers have employed well-dispersed nano-materials to

fill in the gel pores of cement-based materials, to block the transport channels of fluids [9]. Oltulu et al. found that mortar was highly permeation resistant after the addition of nano-silica and nano-alumina, due to the pore structure was optimized and the interface transition zone between cement paste and aggregate was enhanced [10]. Zhang et al. also concluded the positive effect of nano-silica on the resistance of chloride penetration in concrete, and they stated that the incorporation of carbon nanotubes was even more effective [11]. Recently, smart polymers, which are highly controllable, reversible, and responsive to the external stimuli, have raised extensive attention. Intelligent adjustments of fluids transport can be achieved by the introduction of smart polymers, relying on their conformational transformations due to the change in the parameters of pH, temperature, light or redox potentials [11–15]. It may give birth to comprehensive applications in the fields of materials science and life science [15–23]. The temperature-sensitive polymers are the most commonly used. After

* Corresponding authors.

E-mail addresses: tomaszy@seu.edu.cn (Y. Zhou), hlchang@sdu.edu.cn (H. Chang).

¹ School of Materials Science and Engineering, Southeast University, Nanjing 211189, China.

² School of Qilu Transportation, Shandong University, Jinan 250002, China.

³ C-S-H: calcium silicate hydrate, the main hydration product of ordinary Portland cement. ²MD: molecular dynamics, a force field-based numerical computation method. ³TR: transport inhibitor, an admixture to limit the rapid transport of chlorides through concrete.

the modifications of poly(phenylene ether) or poly(ethylene oxide) on the surface of nano-channels, the switch of the channels can be tunable by the temperature control [24]. Besides, Zhang et al. concluded that the nano-channel possessed ultrahigh ionic rectification and highly efficient selective ionic gating, after the addition of septuplet monomers which are sensitive to the concentration of calcium ions [24,26]. Furthermore, the flow transport can also be regulated by the modifications of either interfacial frictions [27] or external pressure [28].

However, the detailed nano-interaction mechanisms still remain unclear due to the difficulties in experimental characterization at such a small length scale. Molecular dynamics (MD), a numerical computation tool based on force fields, can provide significant insights into the physical properties of the solid matrix, the transport features of fluids, the conformational behaviors of organics, and so on [28–32]. It has been successfully applied in the modeling and simulation of fluids transport in the nano-channels of cementitious materials, with the introduction and developments of suitable force fields, e.g., ClayFF [32,34], CSHFF [35], ReaxFF [35,37] force fields. Youssef et al. proposed that the surface of C-S-H nano-pores was hydrophilic due to the orientation effect of non-bridging oxygen atoms on the hydrogen atoms of the interfacial water molecules [38]. By over 150 cases of MD simulation, Qomi et al. concluded that the chemo-physical properties of water in C-S-H gel pores rely on the composition of the matrix [39]. Moreover, Zhou et al. stated that chloride ions can adsorb on the C-S-H surface when confined in the nano-pores of C-S-H, while the adsorption quantity and stability are dependent on the calcium to silicon ratio of the surface [32,40]. Hou's group investigated the capillary penetration process of solutions of NaCl and Na₂SO₄ through the nano-channels of C-S-H by MD simulations, and differentiate the transport features of chlorides and sulfates.[40–43] Furthermore, the interactions between polymers with distinct functional groups (e.g., carboxyl, hydroxyl, alkyl groups) and the C-S-H surface have also been explored by molecular dynamics. It is suggested that high polarity carboxyl groups contribute to the strong adsorption of polymers on C-S-H, while the hydrophobic alkyl groups are not attracted by the surface groups of C-S-H [43–47].

As Mindess pointed out, the typical size range of gel pores in C-S-H is from 0.5 to 10 nm, which highly relates to the transport of water and ions through cement-based materials.[48] Therefore, in this work, we firstly designed a specific polymer structure utilizing molecular dynamics simulations, which can effectively regulate the capillary penetration process in a 6 nm-width nano-channel. Afterward, this polymer was fabricated as a novel ion transport inhibitor and added to the concrete mixtures. Finally, macroscale durability experiments were carried out to test the working effect of this inhibitor.

2. Methods

2.1. Computational methods

2.1.1. Computational model

To simulate the transport process of water and ions through the gel pores of concrete, the model of calcium silicate hydrate, the main hydration product of ordinary Portland cement, is selected as the cementitious matrix. A capillary pore with a width of 6 nm and length of 9 nm is constructed in between two calcium silicate sheets following the methods in Ref.[45], as shown in the right part of Fig. 1. The left part is the bulk fluids, which are constituted of water molecules, sodium ions, and chloride ions. The concentration of Na⁺ and Cl⁻ in the simulation is 0.5 mol/L, approaching the upper limit in the pore solution of marine concrete[49]. Driven by the capillary tension, the fluids will penetrate through the nano-pore of C-S-H, as the common case in concrete [50]. As mentioned above, the polymer, with one hydrophilic carboxyl group at the end and 12 repetitive units of hydrophobic alkyl groups, is simplified as the transport inhibitor. Four pieces of polymer chains are placed on the transport path in the nano-pore of C-S-H, to investigate the effect of inhibitors on the fluids transport. It should be noted that

polymers are located separately in the middle area of the capillary pore before the fluids begin to transport, to avoid the initial adsorption. In total, the computational model owns over 20,000 atoms, to guarantee that simulation results are statistically reliable.

2.1.2. Force fields and simulation details

The ClayFF and CVFF force fields were combined in this work to describe the inorganic and organic system, respectively. ClayFF force field [51] was utilized to depict the interactions between Ca, Si, O, and H atoms in the C-S-H gel. Metal-oxygen interactions are calculated by a Lennard-Jones function and a Coulombic term. The water, hydroxyl, and oxygen-oxygen interactions in the fluids are expressed by the classic single point charge (SPC) model [52]. ClayFF force field has already been used to successfully model the structures of cement hydrates, the interactions between aqueous species and hydrate surface, and the behavior of water and ionic species in the interlayers of calcium silicate hydrate because of the good transferability and reliability [39,53]. On the other hand, the consistent valence force field (CVFF) has been widely utilized in modeling the organic molecules, especially fitted to small carboxylic acids. Structures and binding energies, vibrational frequencies and conformational energies can be accurately calculated using CVFF force field. Besides the Lennard-Jones function and Coulombic term, it also defines the intra-molecular potential, e.g., the energy of deformation of bond lengths, bond angles, torsion angles, and out-of-plane interactions [53,55]. The interaction parameters between organic and inorganic atoms are determined according to the mean rule. Distance parameters are calculated by arithmetic mean rule, while energy parameters are calculated by geometric mean rule [44,56].

The simulations were performed using the LAMMPS software [57], and the periodic boundary condition was applied to all x, y, z-directions of the model. The energy was minimized to eliminate inappropriate atomic coordinates, and subsequently a specific MD simulation procedure was implemented in NVT ensemble. Firstly, a rigid body algorithm was employed to “freeze” the C-S-H matrix, while simultaneously an invisible wall was placed between the inlet of the CSH gel hole and the fluids to prevent the mix of two systems. Afterward, a 2000 ps relaxation simulation was carried out, to ensure a thermodynamic equilibrium for both C-S-H/polymers and the fluids system. Finally, the interface wall at the inlet of the C-S-H gel pore was removed, and the penetration process of fluids into the nano-pore was simulated for another 2000 ps. The Hoover Canonical ensemble (NVT) MD algorithm was used in the simulation, and the time step was 0.001 ps, the temperature was 298 K. During the whole process, thermodynamic information such as pressure, temperature, and energy of the system was monitored to verify the stability of the system and the rationality of the model. The trajectories, displacements, and positions of x, y, z coordinates of all atoms were collected every 0.1 ps for molecular structure, dynamics and interface analysis.

2.2. Experimental methods

2.2.1. Materials

The main binding material for the concrete samples was the P·O 42.5 ordinary portland cement from Conch Cement Company, and its strength at 3 days and 28 days was 27.2 MPa, and 46.6 MPa, respectively. Besides, Class II fly ash and Class S95 mineral powder were used as the mineral admixture. The aggregates include a fine one, which is the river sand with a fineness modulus of 2.45, and a course type, the continuously graded basalt rubble. The SBT® PCA-I from Sobute New Materials Company was employed as the water-reducing admixture, with a 25% water-reducing ratio and an 18% solid content. A carboxylic acid with 12 repetitive units of methyl groups and one carboxyl group was chosen as the precursor of the ion transport inhibitor. It was light yellow and had a pH ≈ 9.

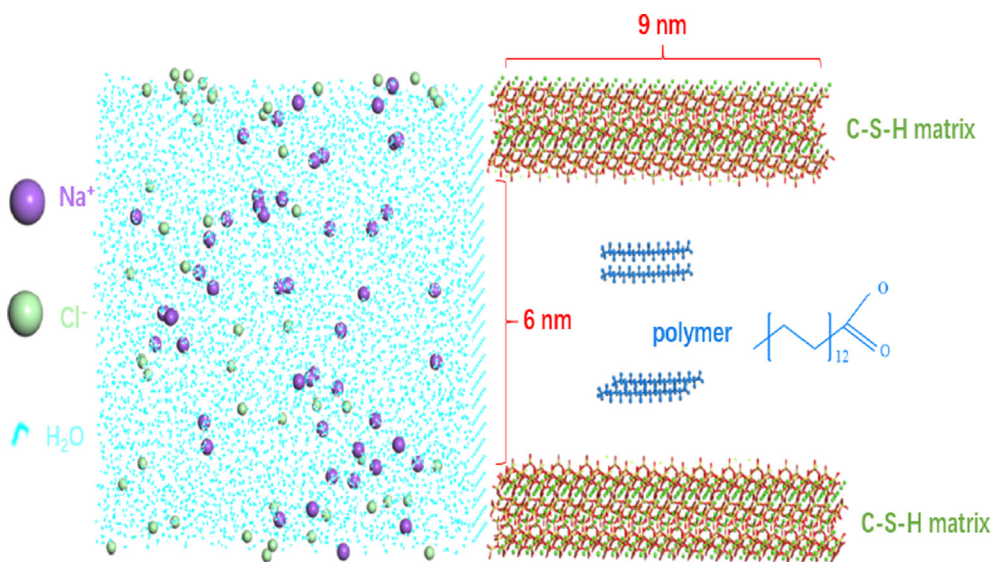


Fig. 1. Schematic illustration of the computational model (the left part denotes the fluids to transport: light blue lines denote water molecules, light green balls denote chloride ions, purple balls denote sodium ions, the right part denotes the nano-pore of C-S-H matrix: green balls denote calcium ions, red and yellow sticks denote silicate tetrahedra, polymer chains are in blue).

2.2.2. Synthesis and testing

The ion transport inhibitor was synthesized according to the following procedures. Firstly, the carboxyl acid was added into the organic solvent of methylbenzene, and the mixture was stirred until homogenized. Subsequently, the organic solution was heated to 50–150 °C. Finally, the product was obtained by mixing a proper amount of polyether and catalyst with the solution and allowing the reaction for 10–16 h.

Four groups of concrete mixtures were prepared using the proportions in Table 1, with the dosage of the ion transport inhibitor varying from 0 to 0.9% (mass ratio of the inhibitor to binding materials). For each group, six core specimens with the size of $\Phi 75 \text{ mm} \times 75 \text{ mm}$ were measured for the water adsorption amount, while three core ones with the size of $\Phi 100 \text{ mm} \times 50 \text{ mm}$ were tested for chloride migration coefficients. The former measurements were referred to BS1881: Part122:1983 [58] to obtain the water adsorption amount of concrete at 0.5 h, 1 h, 2 h, 4 h, 6 h, and 12 h. The chloride migration coefficients were calculated after immersing concrete mixtures into a chloride salt solution for 56 days and then testing the chloride concentration at each depth, according to AASHTO T259 [59].

3. Results and discussions

3.1. Molecular dynamics simulation

Molecular dynamics simulations were employed to design smart polymers with a suitable chemical structure to regulate the capillary penetration in nano-channels. Here, in order for system simplification, calcium silicate hydrate (C-S-H), the main hydration product of ordinary Portland cement, was chosen as the concrete matrix, and a 6-nm-width and 9-nm-length capillary pore in C-S-H was modeled as the transport path of fluids. Smart polymers were placed in the middle area of the nano-channels as the transport inhibitors.

Table 1
Mix proportions of concrete ($\text{kg}\cdot\text{m}^{-3}$).

Number	Cement	Mineral powder	Fly ash	Fine aggregate	Course aggregate	Water	Water reducing admixture	Ion transport inhibitor
1	210	110	110	732	1098	150	4.8	0
2	210	110	110	732	1098	150	4.8	0.3%
3	210	110	110	732	1098	150	4.8	0.6%
4	210	110	110	732	1098	150	4.8	0.9%

3.1.1. Configurations of polymers in an anhydrous C-S-H nano-pore

Before the penetration of fluids into the nano-pores, polymers of transport inhibitor, which are already present in the nano-pore of C-S-H, exhibit strong adsorption configurations on the surface of C-S-H. As shown in Fig. 2a, the polymer chains are either curled up or straightforward in the vicinity of C-S-H surface, with oxygen atoms from the functional groups $-\text{COO}^-$ coordinated with the calcium ions from the C-S-H surface. The intensity distribution of calcium ions from C-S-H, oxygen and carbon atoms from polymers along z-direction, is illustrated in Fig. 2b. As the common structure of C-S-H, large numbers of calcium ions occur in the upper and lower surface of C-S-H [4,60], creating two pieces of major calcium peaks. The peaks of oxygen atoms locate nearby, almost overlapping with calcium peaks, while those of carbon atoms appear farther towards the nano-pore region. It indicates oxygen atoms are closer to the C-S-H surface and contribute to the adsorption of polymers. The radial distribution function shown in Fig. 2c further proves it. For the pair of calcium ions and oxygen atoms, there is a strong intensity peak located at the distance of around 2.3 Å, which means the two species coordinate each other at that distance, and the pairs composed of calcium ions and oxygen atoms exist stably at the interfaces. It corresponds to the snapshot in Fig. 2a. Previous studies have also confirmed this both experimentally and theoretically, in that polymers with high polarity functional groups $-\text{COO}^-$ can strongly adsorb on the C-S-H surface due to the attraction effect between calcium ions from C-S-H and oxygen atoms from $-\text{COO}^-$ [44,47,56].

3.1.2. Transport process of fluids

The bulk fluids outside can penetrate the gel pore automatically due to the capillary penetration effect [60,62]. The penetration processes of fluids into the gel pore with/without transport inhibitors are compared in Fig. 3. The fluids composed of water molecules, sodium, and chloride ions gradually migrate from the bulk solution into the nano-pore as the simulation time goes up. Obviously, the advancing frontier of fluids is not absolutely perpendicular to the C-S-H matrix. Apart from the bulk fluids, a small fraction of water molecules penetrates deeper, located in

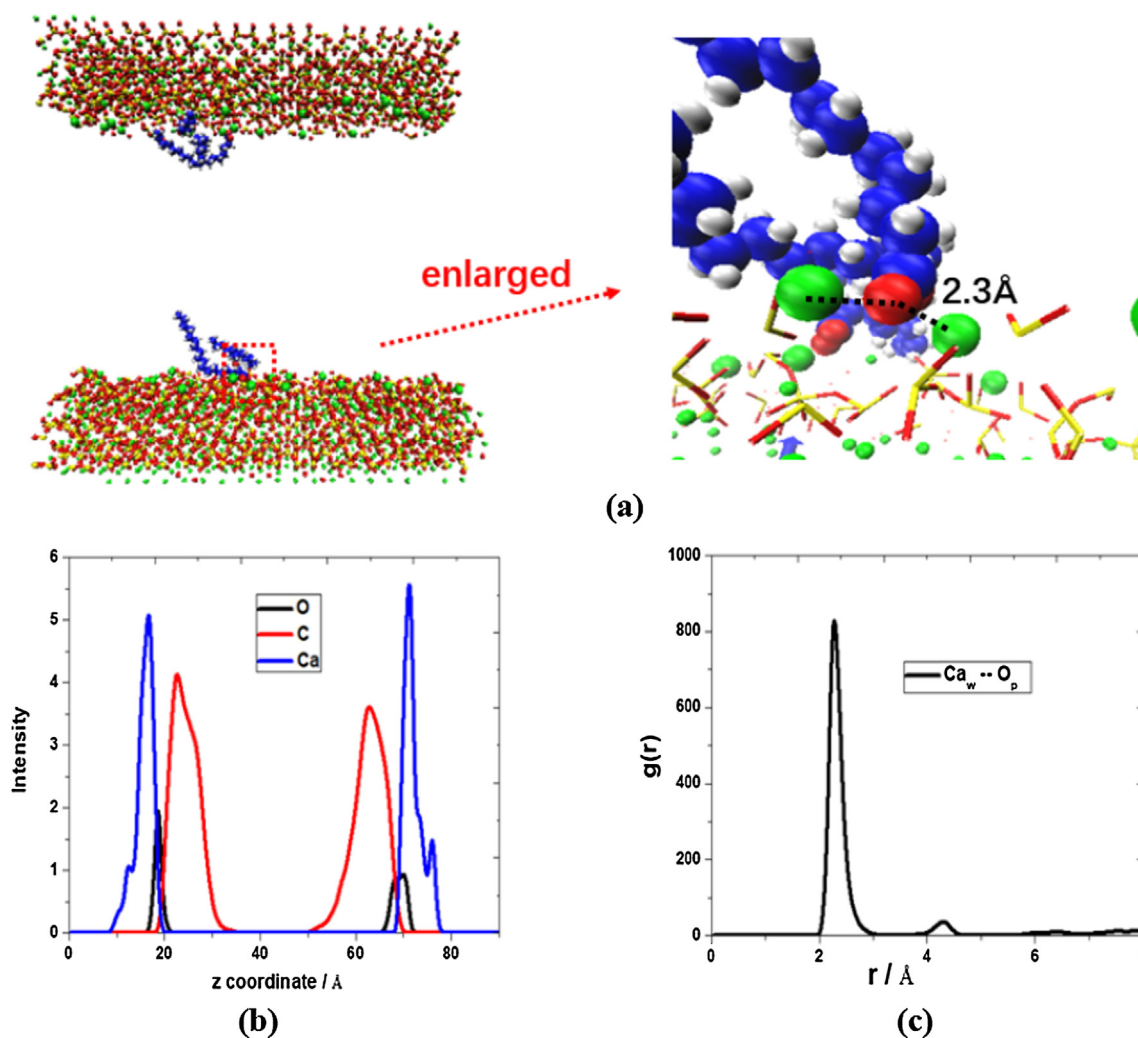


Fig. 2. Interactions between polymers and C-S-H. (a) snapshots of polymer adsorption on C-S-H surface (blue, red and white balls denote the carbon, oxygen, and hydrogen atoms of polymers, green balls denote the calcium ions of C-S-H, red and yellow sticks denote the silicate tetrahedra of C-S-H). (b) the intensity distribution of oxygen, carbon atoms from polymers, and calcium ions from C-S-H long z-direction. (c) the radial distribution function of calcium from C-S-H and oxygen from functional groups of polymers.

the vicinity of the upper and lower surface, creating an arc-shape frontier. It suggests the C-S-H surface is hydrophilic. The frontier shape gets sharper as the penetration proceeds, following a molecular-kinetic theory [63].

In order for a more clear comparison between the two penetration process (gel pore without transport inhibitors – REF, gel pore with transport inhibitor – TR), the penetration depth of fluids into the gel pore as a function of simulation time is recorded in Fig. 4a. During the first 50 ps when the advancing fluids have not reached the polymer position, no differences take place between the two processes, and the profiles of penetration depth almost overlap. However, the fluids migration rate sharply slows down upon the contact with transport inhibitors. As observed in Fig. 3, at 300 ps the advancing frontier in the nano-pore with TR obviously falls behind. In Fig. 4a, it also shows that the slope of TR dramatically decreases after 50 ps, leading to an increasing gap in the penetration depth between TR and REF. At 300 ps, the difference in the penetration depth is around 12 Å. As the simulation proceeds, the polymers keep preventing the penetration of fluids. At 500 ps the penetration frontier in REF is around 20 Å ahead of that in TR, while at 1000 ps the penetration depth in REF is approximately 30 Å larger.

This fluids transport inhibiting effect can be attributed to the hydrophobic functional groups $-\text{CH}_3$ from polymers. This transport

inhibitor has a special molecular structure, with a hydrophilic carboxyl group attracted by the C-S-H surface, and hydrophobic alkyl groups preventing the migration of water molecules. As shown in Fig. 3b, the hydrophilic end of polymer strongly adsorbs on the C-S-H surface, allowing the long chains of hydrophobic alkyl groups in contact with the fluids. Since no fluids are able to go through the alkyl groups, this polymer configuration is equivalent to block the nano-pore, and decrease the width of the transport channel. Furthermore, based on the features and dynamics theory of capillary transport [61,63], fluids located in the middle part of the channel where alkyl groups are absent still cannot penetrate any farther until fluids in the vicinity of C-S-H surface move past polymers.

The mean square displacements (MSD) can reflect the dynamics information of atoms and molecules [39,53], to support the analysis of the fluids penetration process. MSD can be calculated according to the following equation:

$$\text{MSD} = |\mathbf{r}_i(t) - \mathbf{r}_i(0)|^2 \quad (1)$$

where $\mathbf{r}_i(t)$, $\mathbf{r}_i(0)$ represent the position of atom i at time t and origin position respectively. Fig. 4b shows the MSD evolution of water molecules in the REF and TR along the advancing direction (y-axis). Overall, the MSD values of water molecules in REF proportionally increase with the simulation time, implying a stable migration process. For water

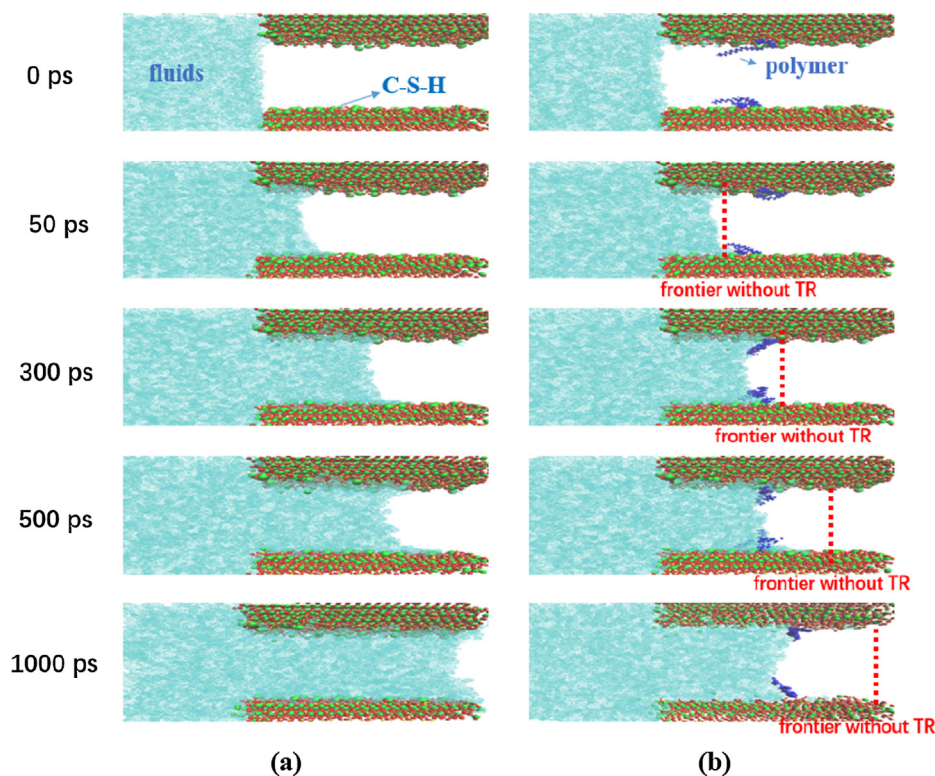


Fig. 3. The snapshots of transport process of fluids into the gel pores (a) without (b) with transport inhibitors (the light blue dots denote fluids, green and red balls denote the upper and lower surface of C-S-H matrix, dark blue chains denote polymers).

molecules in TR, the MSD values in the beginning (0–50 ps) almost overlap with those in REF. Subsequently, the rising rate of MSD in TR becomes lower than that in REF, which indicates the migration of water molecules is inhibited. The difference in MSD values between REF and TR keeps going up, and the final value in TR is around 2000 \AA^2 , only one-third of that in REF. It means the transport of water molecules in the nano-pore of C-S-H is highly affected by the polymers.

The time-dependent density maps of water molecules along the migration direction during the REF and TR penetration process are plotted in Fig. 4c and Fig. 4d, respectively. For REF, it shows that the saturation degree of the gel pore goes up as the water penetration proceeds. After the simulation time of 1250 ps, the whole gel pore is full of water molecules, with a uniform density of 1 g/cm^3 . Prior to the full saturation condition, there is an obvious transition zone with density values varying from 0 to 1 g/cm^3 , as marked by the white dashed lines. It is caused by the arc-shaped advancing frontier, where water molecules only exist near the upper and lower surface of C-S-H. The width of transition area increases with the penetration depth due to the lower contact angle and sharper arc-shape [41]. For TR, the penetration rate of water molecules is obviously slower, and the gel pore is still unsaturated at the simulation time of 2000 ps. It should be noted that the penetration depth of the bulk fluids (density $\approx 1 \text{ g/cm}^3$) experiences no substantial increase from around 500 ps to 2000 ps. In contrast, as shown in Fig. 4d, there is a huge rise in the width of the transition zone simultaneously. It means that due to the inhibiting effect of polymers, only water molecules in the vicinity of C-S-H surface are able to penetrate deeper during that simulation time, while the bulk water molecules fail to move farther. It contributes to a sharper shape of the advancing frontier and a wider transition zone in the density map.

The chloride ions are also the key components of the fluids on top of water molecules, and the penetration process of chlorides is illustrated in Fig. 5. As shown in Fig. 5a, the evolution of the penetration depth of chlorides in REF is similar to that of water molecules, except for minor fluctuations. At the beginning of the simulation time, the profiles of REF and TR almost overlap, which suggests a synchronous migration.

Subsequently, a platform occurs in the TR curve, indicating that the ions transport was strongly inhibited by the polymers. The MSD profiles in Fig. 5b also prove this. The growth of MSD values of chloride ions in TR gradually fall behind that in REF after a proportional increase during the first 50–100 ps, and the gap in between keeps rising. The final MSD value of chlorides in TR at 1500 ps is around 2000 \AA^2 , only one-third of the MSD value of chlorides in REF, which also means the inhibiting effect of polymers on ions transport. Fig. 5c and Fig. 5d describe the density maps of chlorides during the penetration process in REF and TR, respectively. Overall, the chlorides are uniformly distributed along the migration direction during the whole penetration process, and at around 1300 ps the advancing frontier of chloride ions have arrived at the end of the 9 nm-length nano-pore without polymers. However, the polymers, adsorbing at the surface of C-S-H, highly inhibit the transport of chlorides. In Fig. 5d, the penetration depth of chlorides stabilizes at 50–60 \AA from the simulation time of 800 ps to 2000 ps, which corresponds to the case of bulk water molecules in Fig. 4d. It implies that most chlorides at the advancing frontier situate at the bulk fluids rather than minor fluids at the upper and lower surface of C-S-H, and the migration of these chlorides is blocked along with water molecules by transport inhibitors. Moreover, the distribution of chlorides along the penetration direction in TR is still relatively uniform in spite of the inhibited transport.

3.1.3. Configurations of polymers during the fluids transport process

Polymers with one hydrophilic end adsorbing on the surface of C-S-H reply on other hydrophobic groups to highly slow down the fluid transport in the gel pore. The configurations of polymers during the fluids penetration process are illustrated in Fig. 6. A parameter of gyration radius is employed to evaluate the conformation and orientation of polymers [64] and to further elucidate the transport inhibiting mechanism. Here, we consider the components R_y , R_x , R_z of gyration radius, which denote the average space occupied by polymers along y (fluids transport direction), x and z-axis (perpendicular to the fluids transport direction) respectively, given by following equations:

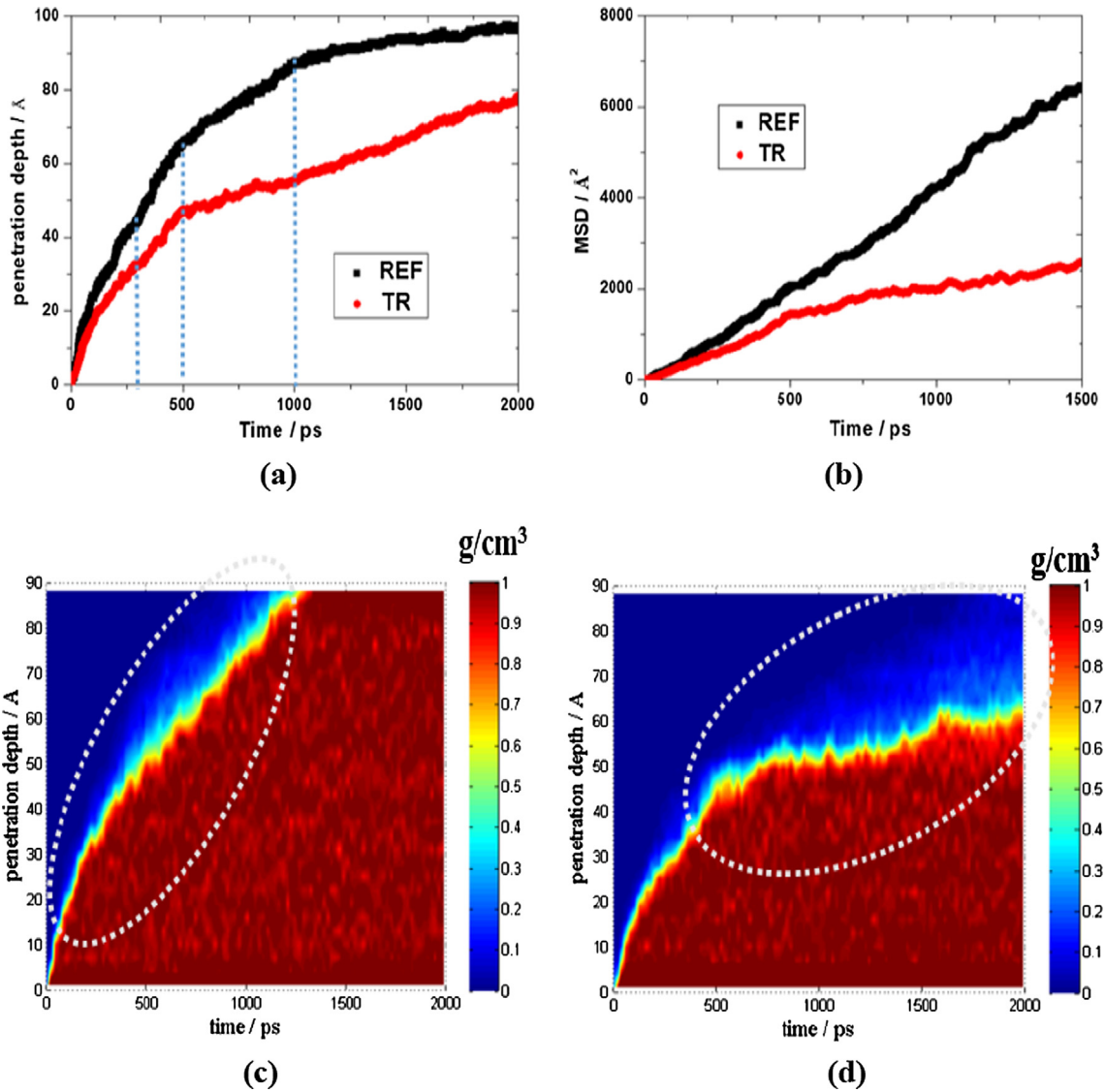


Fig. 4. Transport process of water molecules. (a) penetration depth as a function of simulation time. (b) mean square displacements as a function of simulation time. Density maps along with penetration depth in the nano-pore (c) without transport inhibitors (d) with transport inhibitors.

$$R_x^2 = \left\langle \frac{1}{N} \sum_{i=1}^N (x_i - x_{com})^2 \right\rangle \quad (2)$$

$$R_y^2 = \left\langle \frac{1}{N} \sum_{i=1}^N (y_i - y_{com})^2 \right\rangle \quad (3)$$

$$R_z^2 = \left\langle \frac{1}{N} \sum_{i=1}^N (z_i - z_{com})^2 \right\rangle \quad (4)$$

where N is the number of atoms the polymers, and $(x_{com}, y_{com}, z_{com})$ is the coordinate of geometric center of polymers, (x_i, y_i, z_i) is the coordinate of the i -th atom of polymers, $\langle \cdot \rangle$ denotes the average for all the trajectories during 2000 ps. The greater value of gyration radius indicates polymers occupy more space along this direction.

The snapshots projected on the y - z plane and x - z plane during the fluids transport process are recorded in Fig. 6, and the corresponding gyration radius at each moment is calculated. It can be observed that in the cross-section of the fluids transport (x - z plane), polymer chains always exhibit straight and unfolded conformations, occupying through the entire nano-channel along x -axis. It allows the hydrophobic alkyl groups in full contact with the fluids and prevents their advancing. Polymers act as walls on the migration path of fluids, block the channel

of the C-S-H gel pore, and inhibit the fluids transport. Furthermore, the varying polymer conformations in y - z plane projections suggest that upon contact with the fluids, polymers tend to take up more space along z -direction. The gyration radius along z -direction transforms from 1.14 Å to 3.40 Å, and polymer chains on y - z plain gradually stand vertical to the surface plane of C-S-H. On the contrast, there is a downward trend for the gyration radius along with the fluids advancing direction, which means polymers take up less length space along y -axis. It suggests the height of blocking walls is becoming larger, and the transport inhibiting efficiency tends stronger. At the simulation time of 800 ps (see Fig. 6c), polymers show completely upright configurations. It means polymer chains occupy the largest area in the cross-section of the fluids advancing, forming the highest blocking wall and thus inhibit the transport to the largest degree. Theoretically, according to the classic Lucas-Washburn equation $h^2 = \frac{c \cdot r \cdot \sigma \cos \theta - t}{2\eta}$ (c denotes the form factor of the capillary pore, r denotes the capillary radius, σ denotes the surface tension of fluids, η denotes the viscosity of fluids, θ denotes the contact angle, t denotes the time, and h denotes the penetration depth of fluids) [61,65], as the capillary radius decreases, the penetration depth will also go down in a given time interval. This can explain the stagnation of the bulk fluids transport from 500 ps to 2000 ps, as mentioned earlier.

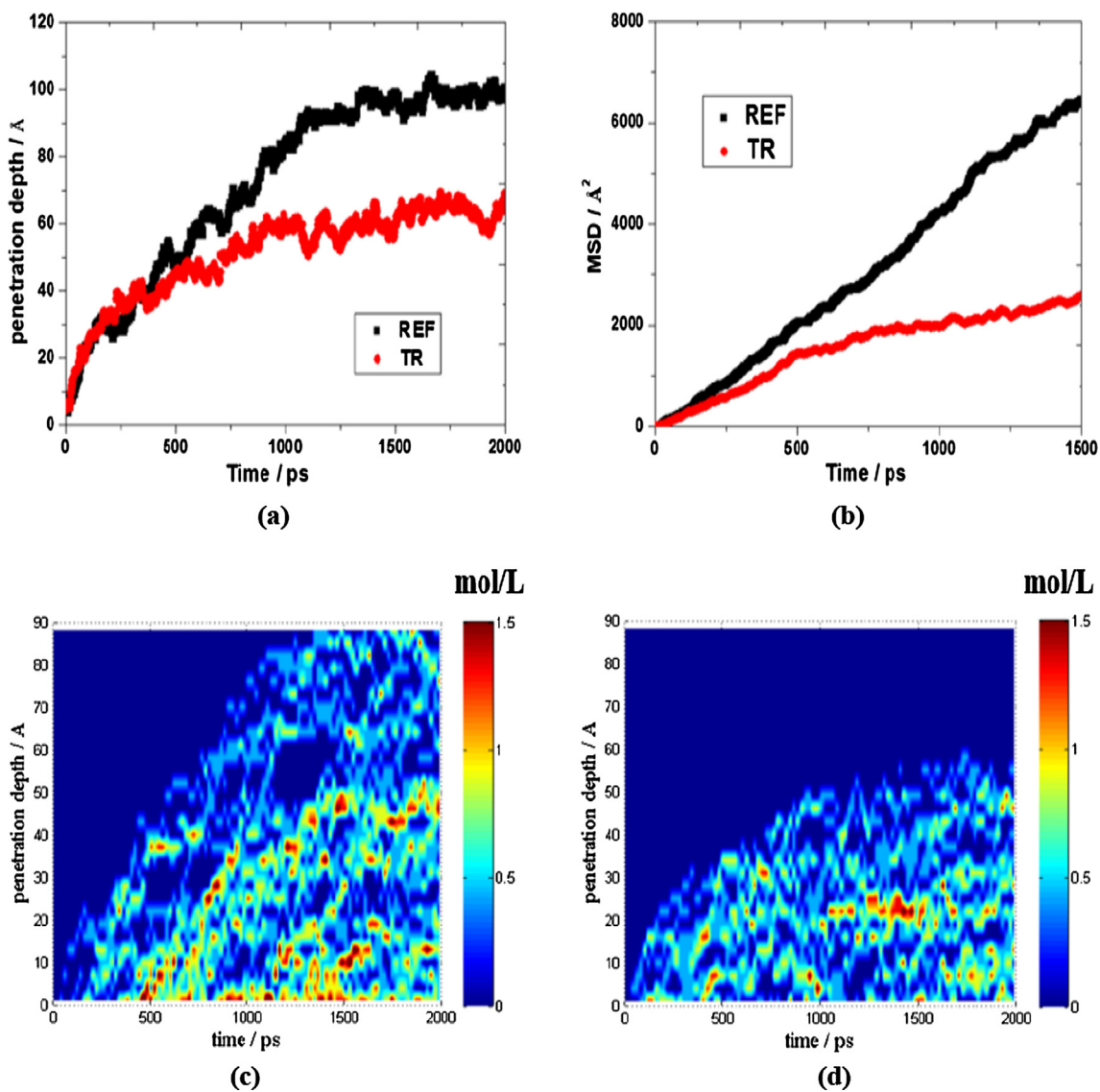


Fig. 5. Transport process of chloride ions. (a) penetration depth as a function of simulation time. (b) mean square displacements as a function of simulation time. Density maps along with penetration depth in the nano-pore (c) without transport inhibitors (d) with transport inhibitors.

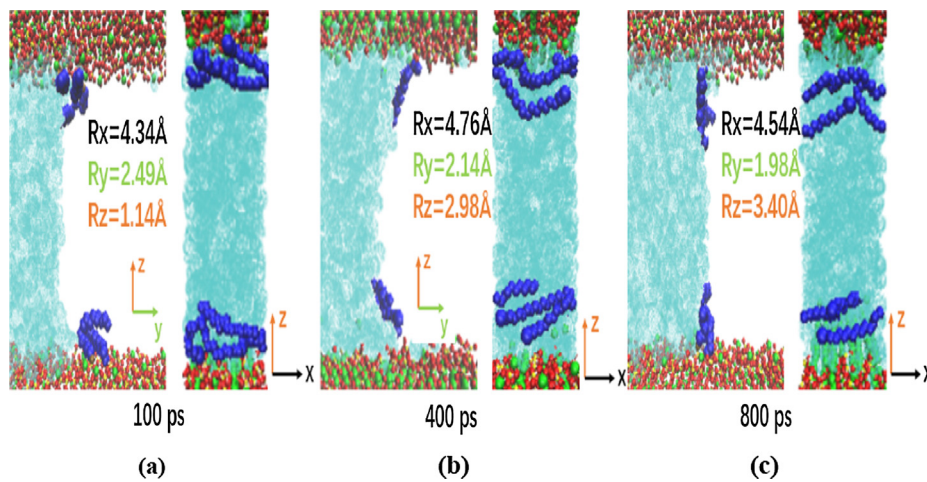


Fig. 6. The snapshots of the system projected on z-y and z-x plane, respectively, and the configuration evolution of polymer chains during the fluids transport process at (a) 100 ps, (b) 400 ps, (c) 800 ps.

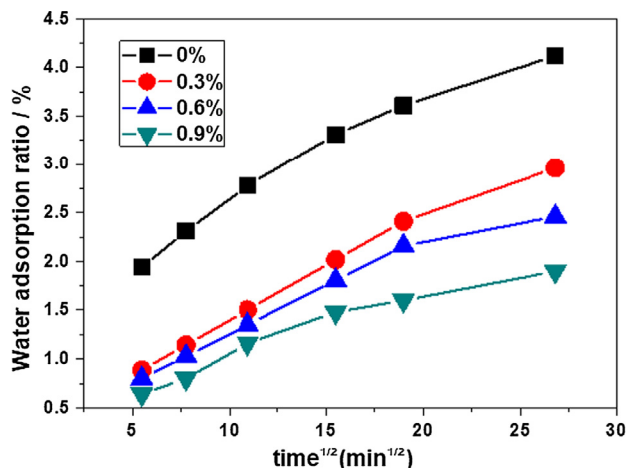


Fig. 7. The evolutions of water adsorption ratios of concrete mixtures with different dosage of ion transport inhibitors.

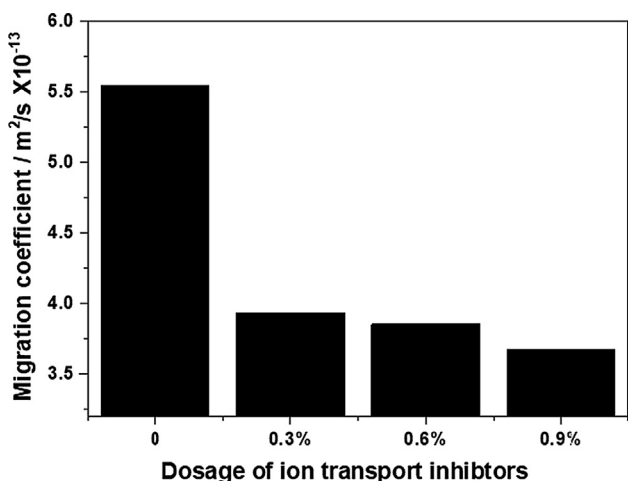


Fig. 8. The chloride migration coefficients of concrete mixtures as a function of the dosage of ion transport inhibitors.

It should be noted that the aggregation effect of polymers cannot be ignored. Previous publications have proved that in the confined nanopores of C-S-H polymer chains intertwined with each other to different degrees, depending on the polarity of functional groups, the concentration, and chemical structure of polymers [43,45]. It is predicted that in this work higher concentration of polymers may also induce a polymer aggregation in the vicinity of C-S-H surface, due to the attractions between carboxyl groups from different polymer chains [45]. Smart Polymer chains entangle with each other, which will decrease the effective contact area with fluids, thus causing a lower inhibiting efficiency on the fluids transport.

3.2. Experiments

Based on the polymer structure proposed by MD simulations, a novel ion transport inhibitor was fabricated and added into the concrete mixtures. Macroscale durability experiments were carried out to test the real effect of inhibitors. Evolutions of water adsorption ratios of concrete mixtures with the increase of immersing time are shown in Fig. 7. The value of the original measurement point (5.5 min^{1/2}) is 1.9% for the concrete with no ion transport inhibitors, while the incorporation of TR dramatically decreases it to 0.6%~0.8%. For each group of the concrete mixtures, the values of water adsorption ratios keep going up as the immersing proceeds. However, the presence of TR significantly slows down the rising rate, and the higher dosage leads to

lower water adsorption ratios. At the last measurement point (26.8 min^{1/2}), the water adsorption ratio of the sample without TR is over 4%, while the mixture with 0.9% dosage of TR only reaches around 1.7%. It proves that the addition of TR effectively inhibits the transport of water through the pores of concrete and thus decreases the water adsorption amount.

The chloride migration coefficient is a key parameter that more directly relevant to the durability of the reinforced concrete structures, and the measurement data of concrete mixtures after immersing for 56 days is given in Fig. 8. It shows that the sample without TR has a high migration coefficient of $5.5 \times 10^{-13} \text{ m}^2/\text{s}$. However, the incorporation of TR decreases the value to lower than $4 \times 10^{-13} \text{ m}^2/\text{s}$. Similarly, the higher dosage has a better performance, which implies the presence of TR effectively slows down the penetration of chloride ions throughout the pores of concrete and may contribute to longer service life.

4. Conclusions

A novel ion transport inhibiting material was designed, fabricated and tested in this work. Molecular dynamics simulations were employed to determine a suitable chemical structure of smart polymers to regulate the capillary penetration of fluids, while experiments were carried out to test the real inhibiting effect of polymers on the transport of water and chloride ions in the porous cementitious matrix.

The designed smart polymer should own one hydrophilic ($-\text{COO}^-$) end and large numbers of hydrophobic (alkyl) groups. On the one hand, the carboxyl group ensures the stable adsorption on the surface of C-S-H, due to the strong electrostatic attraction between high polarity oxygen atoms (from $-\text{COO}^-$) and calcium ions (from C-S-H surface). On the other hand, hydrophobic chains help prevent the transport of fluids. In such a scenario, as fluids were advancing in a gel pore of C-S-H, smart polymer chains, with one end adsorbing on the matrix surface, gradually stood perpendicular to the matrix, which blocked the channel and decreased the cross-sectional area of a transport path. Therefore, the penetration depth and mean square displacements of bulk water molecules and chloride ions were dramatically decreased, as compared with the free capillary penetration process.

Based on the interaction mechanisms among C-S-H matrix, fluids, and organics elucidated above, smart polymers were made into ions transport inhibitors and added to the concrete mixtures. The experimental results prove that the water adsorption amount and chloride ion migration rate of concrete samples experience a huge decrease, indicating the high efficiency of the ion transport inhibitor and substantial enhancement in the durability of reinforced concrete structures.

Acknowledgments

The authors acknowledge the financial support from the National Natural Science Foundation of China (Grant Nos: 51908119, U1706222, 6512009004A), and the Natural Science Foundation of Jiangsu Province (Grant Nos: BK20190367, BK20160104).

References

- [2] K.Y. Ann, H.W. Song, Chloride threshold level for corrosion of steel in concrete, *Corros. Sci.* (2007), <https://doi.org/10.1016/j.corsci.2007.05.007>.
- [3] S. Guzmán, J.C. Gálvez, J.M. Sancho, Cover cracking of reinforced concrete due to rebar corrosion induced by chloride penetration, *Cem. Concr. Res.* (2011), <https://doi.org/10.1016/j.cemconres.2011.04.008>.
- [4] A.J. Allen, J.J. Thomas, H.M. Jennings, Composition and density of nanoscale calcium-silicate-hydrate in cement, *Nat. Mater.* 6 (2007) 311–316, <https://doi.org/10.1038/nmat1871>.
- [5] I.G. Richardson, The calcium silicate hydrates, *Cem. Concr. Res.* 38 (2008) 137–158, <https://doi.org/10.1016/j.cemconres.2007.11.005>.
- [6] M.J. Abdolhosseini Qomi, K.J. Krakowiak, M. Bauchy, K.L. Stewart, R. Shahsavari, D. Jagannathan, D.B. Brommer, A. Baronnet, M.J. Buehler, S. Yip, F.J. Ulm, K.J. Van Vliet, R.J.M. Pellenq, Combinatorial molecular optimization of cement hydrates, *Nat. Commun.* (2014), <https://doi.org/10.1038/ncomms5960>.

- [7] Q. Liu, G. Feng, J. Xia, J. Yang, L. Li, Ionic transport features in concrete composites containing various shaped aggregates: a numerical study, *Compos. Struct.* (2018), <https://doi.org/10.1016/j.compstruct.2017.03.088>.
- [8] H. Chang, P. Feng, K. Lyu, J. Liu, A novel method for assessing C-S-H chloride adsorption in cement pastes, *Constr. Build. Mater.* 225 (2019) 324–331, <https://doi.org/10.1016/j.conbuildmat.2019.07.212>.
- [9] J. Liu, S. Mu, J. Cai, Q. Jiang, Preparation and performance evaluation of cement hydration responsive nanomaterial, *J. Build. Struct.* 1 (2019) 181–187.
- [10] M. Oltulu, R. Şahin, Single and combined effects of nano-SiO₂, nano-Al₂O₃ and nano-Fe₂O₃ powders on compressive strength and capillary permeability of cement mortar containing silica fume, *Mater. Sci. Eng., A* (2011), <https://doi.org/10.1016/j.msea.2011.05.054>.
- [11] M.H. Zhang, H. Li, Pore structure and chloride permeability of concrete containing nano-particles for pavement, *Constr. Build. Mater.* (2011), <https://doi.org/10.1016/j.conbuildmat.2010.07.032>.
- [12] A.A.A.A. Alrashed, O.A. Akbari, A. Heydari, D. Toghraie, M. Zarringhalam, G.A.S. Shabani, A.R. Seifi, M. Goodarzi, The numerical modeling of water/FMWCNT nanofluid flow and heat transfer in a backward-facing contracting channel, *Phys. B Condens. Matter.* (2018), <https://doi.org/10.1016/j.physb.2018.02.022>.
- [13] F. Pourfattah, M. Motamedian, G. Sheikhzadeh, D. Toghraie, O. Ali Akbari, The numerical investigation of angle of attack of inclined rectangular rib on the turbulent heat transfer of water-Al₂O₃ nanofluid in a tube, *Int. J. Mech. Sci.* (2017), <https://doi.org/10.1016/j.ijmecsci.2017.07.049>.
- [14] E. Khodabandeh, M. Bahiraei, R. Mashayekhi, B. Talebjedi, D. Toghraie, Thermal performance of Ag–water nanofluid in tube equipped with novel conical strip inserts using two-phase method: Geometry effects and particle migration considerations, *Powder Technol.* (2018), <https://doi.org/10.1016/j.powtec.2018.06.038>.
- [15] M. Hemmat Esfe, H. Hajmohammad, D. Toghraie, H. Rostamian, O. Mahian, S. Wongwises, Multi-objective optimization of nanofluid flow in double tube heat exchangers for applications in energy systems, *Energy.* (2017), <https://doi.org/10.1016/j.energy.2017.06.104>.
- [16] Q. Zhang, Z. Zhang, H. Zhou, Z. Xie, L. Wen, Z. Liu, J. Zhai, X. Diao, Redox switch of ionic transport in conductive polypyrrole-engineered unipolar nanofluidic diodes, *Nano Res.* 10 (2017) 3715, <https://doi.org/10.1007/s12274-017-1585-4>.
- [17] Y. Sun, J. Ma, F. Zhang, F. Zhu, Y. Mei, L. Liu, D. Tian, H. Li, A light-regulated host-guest-based nanochannel system inspired by channelrhodopsins protein, *Nat. Commun.* 8 (2017) 260, <https://doi.org/10.1038/s41467-017-00330-z>.
- [18] X. Hou, H. Zhang, L. Jiang, Building bio-inspired artificial functional nanochannels: from symmetric to asymmetric modification, *Angew. Chem. Int. Ed.* 51 (2012) 2196, <https://doi.org/10.1002/anie.201104904>.
- [19] C. Secker, S.M. Brosnan, R. Luxenhofer, H. Schlaad, Poly(α-peptoids) revisited: synthesis, properties, and use as biomaterial, *Macromol. Biosci.* 15 (2015) 881, <https://doi.org/10.1002/mabi.201500023>.
- [20] V.D. Ta, A. Dunn, T.J. Wasley, J. Li, R.W. Kay, J. Stringer, P.J. Smith, E. Esenturk, C. Connaughton, J.D. Shepherd, Laser textured superhydrophobic surfaces and their applications for homogeneous spot deposition, *Appl. Surf. Sci.* (2016), <https://doi.org/10.1016/j.apsusc.2016.01.019>.
- [21] Z. Dong, Y. Li, Q. Zou, Degradation and biocompatibility of porous nano-hydroxyapatite/polyurethane composite scaffold for bone tissue engineering, *Appl. Surf. Sci.* (2009), <https://doi.org/10.1016/j.apsusc.2009.01.083>.
- [22] A.H. Saeedi, M. Akbari, D. Toghraie, An experimental study on rheological behavior of a nanofluid containing oxide nanoparticle and proposing a new correlation, *Phys. E Low-Dimens. Syst. Nanostruct.* (2018), <https://doi.org/10.1016/j.physe.2018.02.018>.
- [23] M.A. Esfahani, D. Toghraie, Experimental investigation for developing a new model for the thermal conductivity of silica/water-ethylene glycol (40%–60%) nanofluid at different temperatures and solid volume fractions, *J. Mol. Liq.* (2017), <https://doi.org/10.1016/j.molliq.2017.02.037>.
- [24] S.K. Hwang, I. Bae, R.H. Kim, C. Park, Flexible non-volatile ferroelectric polymer memory with gate-controlled multilevel operation, *Adv. Mater.* 24 (2012) 5910, <https://doi.org/10.1002/adma.201201831>.
- [25] Z. Zhang, X.Y. Kong, K. Xiao, G. Xie, Q. Liu, Y. Tian, H. Zhang, J. Ma, L. Wen, L. Jiang, A bioinspired multifunctional heterogeneous membrane with ultrahigh ionic rectification and highly efficient selective ionic gating, *Adv. Mater.* 28 (2016) 144, <https://doi.org/10.1002/adma.201503668>.
- [26] Z. Zhang, G. Xie, K. Xiao, X.-Y. Kong, P. Li, Y. Tian, L. Wen, L. Jiang, Asymmetric multifunctional heterogeneous membranes for pH- and temperature-cooperative smart ion transport modulation, *Adv. Mater.* 28 (2016) 9614, <https://doi.org/10.1002/adma.201602758>.
- [27] Z.Q. Zhang, H.F. Ye, Z. Liu, J.N. Ding, G.G. Cheng, Z.Y. Ling, Y.G. Zheng, L. Wang, J.B. Wang, Carbon nanotube-based charge-controlled speed-regulating nanoclutch, *J. Appl. Phys.* 111 (2012) 114304, <https://doi.org/10.1063/1.4724344>.
- [28] Z.Q. Zhang, H.W. Zhang, L. Wang, Y.G. Zheng, J.B. Wang, Pressure control model for transport of liquid mercury in carbon nanotubes, *Appl. Phys. Lett.* 90 (2007) 144105, <https://doi.org/10.1063/1.2720744>.
- [29] P. Alipour, D. Toghraie, A. Karimipour, M. Hajian, Modeling different structures in perturbed Poiseuille flow in a nanochannel by using of molecular dynamics simulation: Study the equilibrium, *Phys. A Stat. Mech. Its Appl.* (2019), <https://doi.org/10.1016/j.physa.2018.09.177>.
- [30] P. Alipour, D. Toghraie, A. Karimipour, M. Hajian, Molecular dynamics simulation of fluid flow passing through a nanochannel: effects of geometric shape of roughnesses, *J. Mol. Liq.* (2019), <https://doi.org/10.1016/j.molliq.2018.11.057>.
- [31] M. Tohid, D. Toghraie, The effect of geometrical parameters, roughness and the number of nanoparticles on the self-diffusion coefficient in couette flow in a nanochannel by using of molecular dynamics simulation, *Phys. B Condens. Matter.* (2017), <https://doi.org/10.1016/j.physb.2017.05.014>.
- [32] P. Alipour, D. Toghraie, A. Karimipour, Investigation the atomic arrangement and stability of the fluid inside a rough nanochannel in both presence and absence of different roughness by using of accurate nano scale simulation, *Phys. A Stat. Mech. Its Appl.* (2019), <https://doi.org/10.1016/j.physa.2019.04.243>.
- [33] Y. Zhou, D. Hou, J. Jiang, P. Wang, Chloride ions transport and adsorption in the nano-pores of silicate calcium hydrate: Experimental and molecular dynamics studies, *Constr. Build. Mater.* 126 (2016), <https://doi.org/10.1016/j.conbuildmat.2016.09.110>.
- [34] P. Wang, Y. Jia, T. Li, D. Hou, Q. Zheng, Molecular dynamics study on ions and water confined in the nanometer channel of Friedel's salt: Structure, dynamics and interfacial interaction, *PCCP* (2018), <https://doi.org/10.1039/c8cp02450b>.
- [35] D. Hou, H. Ma, Y. Zhu, Z. Li, Calcium silicate hydrate from dry to saturated state: Structure, dynamics and mechanical properties, *Acta Mater.* 67 (2014) 81–94, <https://doi.org/10.1016/j.actamat.2013.12.016>.
- [36] Y. Zhou, D. Hou, G. Geng, P. Feng, J. Yu, J. Jiang, Insights into the interfacial strengthening mechanisms of calcium-silicate-hydrate/polymer nanocomposites, *PCCP* 20 (2018) 8247, <https://doi.org/10.1039/c8cp00328a>.
- [37] D. Hou, T. Zhao, H. Ma, Z. Li, Reactive molecular simulation on water confined in the nanopores of the calcium silicate hydrate gel: structure, reactivity, and mechanical properties, *J. Phys. Chem. C* 119 (2015) 1346–1358, <https://doi.org/10.1021/jp509292q>.
- [38] M. Yousef, R.J.M. Pellenq, B. Yildiz, Glassy nature of water in an ultraconfining disordered material: the case of calcium-silicate-hydrate, *J. Am. Chem. Soc.* 133 (2011) 2499–2510, <https://doi.org/10.1021/ja107003a>.
- [39] M.J.A. Qomi, M. Bauchy, F.J. Ulm, R.J.M. Pellenq, Anomalous composition-dependent dynamics of nanoconfined water in the interlayer of disordered calcium-silicates, *J. Chem. Phys.* 140 (2014), <https://doi.org/10.1063/1.4864118>.
- [40] Y. Zhou, D. Hou, J. Jiang, L. Liu, W. She, J. Yu, Experimental and molecular dynamics studies on the transport and adsorption of chloride ions in the nano-pores of calcium silicate phase: The influence of calcium to silicate ratios, *Micropor. Mesopor. Mater.* 255 (2018), <https://doi.org/10.1016/j.micromeso.2017.07.024>.
- [41] D. Hou, T. Li, P. Wang, Molecular dynamics study on the structure and dynamics of NaCl solution transport in the nanometer channel of CASH Gel, *ACS Sustain. Chem. Eng.* 6 (2018) 9498–9509, <https://doi.org/10.1021/acsschemeng.8b02126>.
- [42] D. Hou, Y. Jia, J. Yu, P. Wang, Q. Liu, Transport properties of sulfate and chloride ions confined between calcium silicate hydrate surfaces: a molecular dynamics study, *J. Phys. Chem. C* 122 (2018) 28021–28032, <https://doi.org/10.1021/acs.jpcc.8b07484>.
- [43] D. Hou, D. Li, J. Yu, P. Zhang, Insights on capillary adsorption of aqueous sodium chloride solution in the nanometer calcium silicate channel: a molecular dynamics study, *J. Phys. Chem. C* (2017), <https://doi.org/10.1021/acs.jpcc.7b04367>.
- [44] Y. Zhou, D. Hou, J. Jiang, W. She, J. Li, Molecular dynamics study of solvated aniline and ethylene glycol monomers confined in calcium silicate nanochannels: a case study of tobermorite, *PCCP* 19 (2017), <https://doi.org/10.1039/c7cp02928d>.
- [45] Y. Zhou, D. Hou, H. Manzano, C.A. Orozco, G. Geng, P.J.M. Monteiro, J. Liu, Interfacial connection mechanisms in calcium-silicate-hydrates/polymer nanocomposites: a molecular dynamics study, *ACS Appl. Mater. Interf.* 9 (2017) 41014–41025, <https://doi.org/10.1021/acsmi.7b12795>.
- [46] J. Yang, D. Hou, Q. Ding, Structure, dynamics, and mechanical properties of cross-linked calcium aluminosilicate hydrate: a molecular dynamics study, *ACS Sustain. Chem. Eng.* (2018), <https://doi.org/10.1021/acssuschemeng.8b01749>.
- [47] A. Picker, L. Nicoleau, A. Nonat, C. Labbez, H. Colfen, Identification of binding peptides on calcium silicate hydrate: a novel view on cement additives, *Adv. Mater.* 26 (2014) 1135–1140, <https://doi.org/10.1002/adma.201303345>.
- [48] S. Mindess, J.F. Young, Concrete, second ed., Prentice Hall PTR, 2003.
- [49] H. Taylor, Cement Chemistry, Thomas Telford, second ed., Thomas Telford Publishing, London, 1997.
- [50] L. Bertolini, B. Elsener, P. Pedferri, E. Redaelli, R.B. Polder, Transport processes in concrete, *Corros. Steel Concr.* (2013), <https://doi.org/10.1002/9783527651696.ch2>.
- [51] R.T. Cygan, J.-J. Liang, A.G. Kalinichev, Molecular models of hydroxide, oxyhydroxide, and clay phases and the development of a general force field, *J. Phys. Chem. B* 108 (2004) 1255–1266, <https://doi.org/10.1021/jp0363287>.
- [52] H.J.C. Berendsen, J.P.M. Postma, W.F. Van Gunsteren, J. Hermans, Interaction models for water in relation to protein hydration, *Internat. Forces.* (1981) 331–342, https://doi.org/10.1007/978-94-015-7658-1_21.
- [53] D. Hou, Z. Li, Molecular dynamics study of water and ions transport in nano-pore of layered structure: a case study of tobermorite, *Micropor. Mesopor. Mater.* (2014), <https://doi.org/10.1016/j.micromeso.2014.04.011>.
- [54] P. Dauber-Osguthorpe, et al., Structure and energetics of ligand binding to proteins: escherichia coli dihydrofolate reductase-trimethoprim, a drug-receptor system, *Proteins* 4 (1988) 31–47, <https://doi.org/10.1002/prot.340040106>.
- [55] H. Holtje, HESSIAN consistent valence force-field parameterization of bond lengths and angles with quantum chemical ab initio methods applied to some heterocyclic dopamine D3-receptor agonists, *J. Comput. Chem.* 19 (1998) 935–946, [https://doi.org/10.1002/\(SICI\)1096-987X\(199806\)19:8<935::AID-JCC12>3.0.CO;2-6](https://doi.org/10.1002/(SICI)1096-987X(199806)19:8<935::AID-JCC12>3.0.CO;2-6).
- [56] F. Sanchez, L. Zhang, Interaction energies, structure, and dynamics at functionalized graphite structure-liquid phase interfaces in an aqueous calcium sulfate solution by molecular dynamics simulation, *Carbon N. Y.* 48 (2010) 1210–1223, <https://doi.org/10.1016/j.carbon.2009.11.044>.
- [57] S. Plimpton, LAMMPS-large-scale atomic/molecular massively parallel simulator, Sandia Natl. Lab, 2007.
- [58] British Standards Institution, Testing concrete Part 122: Method for determination of water absorption, 1983.
- [59] American Association of State Highway and Transportation Officials, Standard

- method of test for resistance of concrete to chloride ion penetration.
- [60] R.J.-M. Pellenq, A. Kushima, R. Shahsavari, K.J. Van Vliet, M.J. Buehler, S. Yip, F.-J. Ulm, A realistic molecular model of cement hydrates, *Proc. Natl. Acad. Sci.* 106 (2009) 16102–16107, <https://doi.org/10.1073/pnas.0902180106>.
- [61] P.K. Mehta, P.J.M. Monteiro, *Concrete Microstructure, Properties, and Materials*, 4th ed., McGraw-Hill Education, 2014.
- [62] E.W. Washburn, The dynamics of capillary flow, *Phys. Rev.* (1921), <https://doi.org/10.1103/PhysRev.17.273>.
- [63] M. Bracke, F. Voegt, P. Joos, The kinetics of wetting: the dynamic contact angle, *Trends Colloid Interf. Sci.* III (2007), <https://doi.org/10.1007/bfb0116200>.
- [64] H. Zhao, Y. Wang, Y. Yang, X. Shu, H. Yan, Q. Ran, Effect of hydrophobic groups on the adsorption conformation of modified polycarboxylate superplasticizer investigated by molecular dynamics simulation, *Appl. Surf. Sci.* 407 (2017) 8–15, <https://doi.org/10.1016/j.apsusc.2017.02.132>.
- [65] L. Hanžič, L. Kosec, I. Anžel, Capillary absorption in concrete and the Lucas-Washburn equation, *Cem. Concr. Compos.* (2010), <https://doi.org/10.1016/j.cemconcomp.2009.10.005>.